Modern Physics Letters B
Vol. 38, No. 25 (2024) 2450226 (11 pages)

DOI: 10.1142/S0217984924502269

World Scientific
www.worldscientific.com

Conductivity in the half-filled disordered Hubbard model: A typical medium dynamical mean-field study

Anh-Tuan Hoang* and Thi-Hai-Yen Nguyen†

Institute of Physics, Vietnam Academy of Science and Technology, Vietnam Graduate University of Science and Technology, Vietnam Academy of Science and Technology, Vietnam
*hatuan@iop.vast.vn
†nhyen@iop.vast.vn

Duc-Anh Le

Faculty of Physics, Hanoi National University of Education, Xuan Thuy 136, Cau Giay, Hanoi 10000, Vietnam
anhld@hnue.edu.vn

Received 1 March 2023
Revised 14 December 2023
Accepted 23 December 2023
Published 28 February 2024

The conductivity for half-filled disordered Hubbard model in different interaction regimes is studied using a typical medium dynamical mean-field theory. The Kubo formula with the geometrically averaged Green function is used to calculate the optical and dc conductivity of the system. The dependence of the conductivities in the model on the random potential and temperature in the weak and intermediate interaction regimes is investigated numerically. It is shown that in the weak interaction regime at a fixed temperature the optical conductivity at low frequencies as well as the dc conductivity get decreased as disorder strength increases. Whereas in the intermediate interaction regime, the results show a reentrant effect of the insulating phases. Our dc conductivity of a non-interacting disordered system is consistent with those known in the literature and our other results are in agreement with the phase diagram obtained by using typical medium theory with different impurity solvers.

Keywords: Conductivity; disordered Hubbard model; typical medium theory.

1. Introduction

The properties of many materials are greatly influenced by the Coulomb interaction between the electrons and lattice disorder. Namely, these two effects are main sources leading to a metal–insulator transitions (MITs): Mott or the correlation-driven MIT and Anderson or disorder-driven MIT. The interplay between

*Corresponding author.

interaction and disorder also can lead to complicated many-body effects that have received much attention.[1–3]

One of the most successful methods for investigating the strongly correlated electron system and Mott MIT is the dynamical mean-field theory (DMFT).[4] However, if the effect of local disorder is taken into account through the arithmetical average of the local density of states (LDOS) it is difficult to distinguish between extended and localized states. Therefore such a theory (the combination of coherent potential approximation with DMFT: CPA-DMFT) cannot accurately capture Anderson localization. Nevertheless, a typical medium theory (TMT), in which the typical density of states is defined as the geometric averaged LDOS, is well suited to describe Anderson localization.[5–10] In Addition, the TMT was successfully employed to study the MIT in the Anderson-Falicov-Kimball (AFK) model and Anderson-Hubbard model (AHM).[6–10] The TMT also used to construct the nonmagnetic phase diagram in mass imbalanced AHM at half-filling as well as in AHM with site-dependent interactions.[11,12]

Most of the previous studies on the influence of correlation and disorder in the half-filled Hubbard model were carried out at zero temperature. In this report, we compute the conductivity in the weak and intermediate interaction regimes of the half-filled Hubbard model with disorder as a function of temperature, which is an important probe of the system. Indeed, the conductivity in the disordered Hubbard model has been studied in Refs. 13–17. However, in Refs. 13, 14 the calculations have been performed away from half-filling in order to avoid the physics of a Mott insulator. In Ref. 15 the conductivity has been investigated on a square lattice by the mean field Monte Carlo (MFMC) technique, where the lattice size is limited while in Refs. 16, 17 a half-filled Hubbard model with disorder in an infinite dimension has been studied with the arithmetically averaged Green function, i.e. the effect of Anderson localization has been not considered. To solve these problems, we use the equation of motion method (EOM) to find the Green function for the effective Anderson impurity model. Like the iterated perturbation theory (ITP), one of the important advantages of EOM is that it can be used directly on the real frequency axis.[18,19] We note that at zero temperature the phase diagram found from TMT-DMFT with the EOM is in good agreement with those obtained by the statistical DMFT[20] as well as the TMT-DMFT using the numerical renormalization group[8] and the four boson technique as an impurity solver.[9]

In Sec. 2, we present our model and theoretical formulation. In Sec. 3, the optical and dc conductivity in the weak and intermediate interaction regimes are calculated and discussed. Finally, Sec. 4 concludes.

2. Theoretical Formulation

The Hamiltonian of the disordered Hubbard model is given by

$$H = -t \sum_{\langle i,j\rangle,\sigma} (a^{+}_{i\sigma} a_{j\sigma} + \text{h.c.}) + \sum_{i,\sigma} (\varepsilon_i - \mu_\sigma) n_{i\sigma} + U \sum_i n_{i\uparrow} n_{i\downarrow}, \tag{1}$$

where the local energies ε_i are random variables with a uniform probability distribution $P(\varepsilon_i) = \Theta(\Delta/2 - |\varepsilon_i|)/\Delta$, where Θ being the step function and Δ being the disorder strength. U is the on-site Coulomb interaction, t and μ are the nearest-neighbor hopping amplitude and the chemical potential, $a_{i\sigma}(a^+_{i\sigma})$ annihilates (creates) an electron with spin σ at site i, $n_{i\sigma} = a^+_{i\sigma}a_{i\sigma}$.

In the TMT-DMFT, the Hamiltonian model in Eq. (1) is mapped onto an ensemble of effective single impurity Anderson model (SIAM) with different local energies ε_i. In this work, we consider the paramagnetic case at half-filling, for which $\langle n_{i\uparrow}\rangle = \langle n_{i\downarrow}\rangle = \langle n_i\rangle/2$ and $\mu = U/2$. The impurity Green function derived from decoupling the equations of motion at the second order takes the following form[18,21]

$$G(\omega,\varepsilon_i) = \frac{1-\langle n_i\rangle/2}{\omega-\varepsilon_i+U/2-\eta(\omega)+U\Pi_1(\omega,\varepsilon_i)[\omega-\varepsilon_i-U/2-\eta(\omega)-\Pi_3(\omega,\varepsilon_i)]^{-1}} + \frac{\langle n_i\rangle/2}{\omega-\varepsilon_i-U/2-\eta(\omega)-U\Pi_2(\omega,\varepsilon_i)[\omega-\varepsilon_i+U/2-\eta(\omega)-\Pi_3(\omega,\varepsilon_i)]^{-1}}, \tag{2}$$

where the "self-energies" Π_i are defined by

$$\Pi_i(\omega,\varepsilon_i) = \int_{-\infty}^{+\infty} dz\,\Gamma(z)\left(\frac{1}{\omega-z}+\frac{1}{\omega-2\varepsilon_i+z}\right)F_i(z). \tag{3}$$

Here, $F_1(z) = f(z)$, $F_2(z) = 1-f(z)$, $F_3(z) = 1$, with $f(z) = (\exp(\frac{z}{T})+1)^{-1}$ being the Fermi-Dirac function; $\Gamma(z) = -\frac{1}{\pi}\Im\eta(z+i0^+)$ and $\langle n_i\rangle = -\frac{2}{\pi}\int dz\, f(z)\,\Im G(z,\varepsilon_i)$. $\eta(z)$ is the hybridization function of a bath surrounding the impurities, which must be determined self-consistently. From Eqs. (2) and (3) the local density of states (LDOS) $\rho(\omega,\varepsilon_i) = -\Im G(\omega,\varepsilon_i)/\pi$ is calculated. Then we obtain the geometrically averaged LDOS $\rho_g(\omega) = \exp[\langle\ln\rho(\omega,\varepsilon_i)\rangle]$ and the arithmetically averaged LDOS $\rho_a(\omega) = \langle\rho(\omega,\varepsilon_i)\rangle$, where $\langle O(\varepsilon_i)\rangle = \int d\varepsilon_i P(\varepsilon_i)O(\varepsilon_i)$ is an arithmetic mean of $O(\varepsilon_i)$. The Hilbert transformation yields the lattice Green function:

$$G_\alpha(\omega) = \int_{-\infty}^{+\infty} d\omega'\,\frac{\rho_\alpha(\omega')}{\omega-\omega'}, \tag{4}$$

where α stands for either "g" or "a", respectively, TMT-DMFT or CPA-DMFT approach. We note that G_α depends on the temperature through n_i and through the "self-energy" Π_1 and Π_2. We use the semielliptic non-interacting density of states (DOS), $\rho_0(z) = 4\sqrt{1-4(z/W)^2}/\pi W$, for which the self-consistent condition for the TMT-DMFT scheme is given by $\eta(\omega) = W^2G_\alpha(\omega)/16$.

From the DMFT self-consistent condition one finds

$$G(\omega,\varepsilon_i) = \int_{-\infty}^{+\infty}\frac{\rho_0(z)dz}{\omega+\mu-\varepsilon_i-z-\Sigma(\omega,\varepsilon_i)}, \tag{5}$$

with the self-energy $\Sigma(\omega, \varepsilon_i)$ defined through the local Dyson equation

$$\Sigma(\omega, \varepsilon_i) = \omega + \mu - \varepsilon_i - \eta(\omega) - \frac{1}{G(\omega, \varepsilon_i)}. \tag{6}$$

For the disordered system, performing the average over the distribution of ε_i from Eqs. (4) and (5) yields the lattice Green function[2,7,8]

$$G_\alpha(\omega) = \int_{-\infty}^{+\infty} \frac{\rho_0(z)dz}{G_\alpha^{-1}(\omega) + \eta(\omega) - z}. \tag{7}$$

Here the two kinds of averages, arithmetic and geometric, can be made. Therefore we obtain two corresponding spectral functions:

$$A_\alpha(\varepsilon, \omega) = -\frac{1}{\pi} \Im\{[G_\alpha(\omega)]^{-1} + \eta(\omega) - \varepsilon\}^{-1}. \tag{8}$$

With the knowledge of the spectral function $A(\varepsilon, \omega)$, the optical conductivity can be determined by using the standard Kubo formula[17,22]

$$\sigma(\omega) = \sigma_0 \int_{-\infty}^{+\infty} d\varepsilon \rho_0(\varepsilon) \int_{-\infty}^{+\infty} d\omega' A(\varepsilon, \omega') A(\varepsilon, \omega' + \omega) F(\omega', \omega), \tag{9}$$

with $\sigma_0 = 4\pi e^2/\hbar$, $F(\omega', \omega) = [f(\omega') - f(\omega' + \omega)]/\omega$. As noted in Ref. 3 that the typical local density of states (TDOS) directly determines the conductivity of electrons, so in Eq. (9) $A_g(\varepsilon, \omega)$ which takes into account only extended states is chosen.[7] However, to clearly study the effect of Anderson localization, we compare some results obtained using TMT-DMFT, $A_g(\varepsilon, \omega)$, with those of CPA-DMFT $A_a(\varepsilon, \omega)$.

The temperature-dependent dc conductivity is obtained from Eq. (9) in the limit $\omega \to 0$

$$\sigma_T = \frac{\sigma_0}{T} \int_{-\infty}^{+\infty} d\varepsilon \rho_0(\varepsilon) \int_{-\infty}^{+\infty} d\omega [A(\varepsilon, \omega)]^2 f(\omega)[1 - f(\omega)]. \tag{10}$$

3. Numerical Results and Discussion

Before performing the conductivity calculations we solve numerically the DMFT equations and build the phase diagram. The TMT-DMFT phase diagram of the AHM at half-filling and at zero temperature $T = 0$ is shown in Fig. 1. In this paper we take the non-interacting bandwidth $W = 1$ as the energy unit. Here as in Ref. 12 the ground state is classified from the obtained values of ρ_a and ρ_g as follows (through this work, the Fermi level is chosen as the origin of the energy axis): (1) $\rho_a(0) \neq 0$ and $\rho_g(0) \neq 0$ specify a metallic phase; (2) $\rho_g(0) = 0$ and $\int \rho_g(\omega) d\omega \neq 0$ give a Mott insulating phase; (3) $\int \rho_g(\omega) d\omega = 0$ indicates an Anderson localized phase. We note that in contrast to Refs. 10–12, where for simplicity we have made the following approximations: $\Pi_1(\omega, \varepsilon_i) = \Pi_2(\omega, \varepsilon_i) = \Pi_3(\omega, \varepsilon_i)/2 = \eta(\omega)$. This approximation is exact at the non-disordered limit and become worse as the disorder strength increases. In order to take into account the missing effect of the disorder due

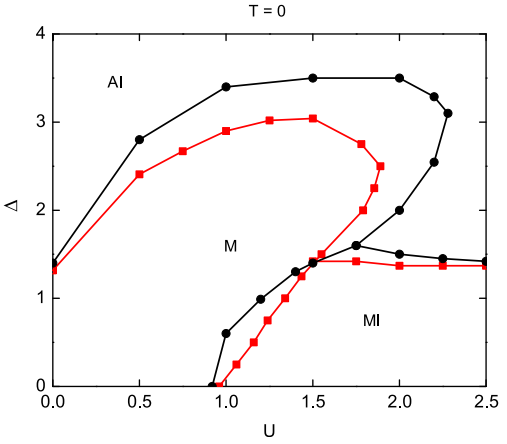

Fig. 1. (Color online) TMT-DMFT (U, Δ) phase diagram for the half-filled disordered Hubbard model at $T = 0$: A comparison between EOM with the "self-energies" Π_i numerically calculated from Eq. (3) (solid line with squares) and the approximations: $\Pi_1(\omega, \varepsilon_i) = \Pi_2(\omega, \varepsilon_i) = \Pi_3(\omega, \varepsilon_i)/2 = \eta(\omega)$ made in Ref. 12 (solid line with dots). M, MI and AI stand for metal, Mott insulator and Anderson insulator, respectively. Energy scale: $W = 1$.

to this approximation in this work the "self-energies" Π_i are numerically calculated from Eq. (3). As a result, the metallic region changes significantly compared to that of Ref. 12, especially for large Δ. From the phase diagram one can distinguish three different interaction regimes regarding the metallic and insulating phase boundaries: (1) weak interaction regime corresponds to $U < U_c(\Delta = 0)$, i.e. $0 < U < \sqrt{3}/2 \approx 0.87$: in this regime for a fixed U only a phase transition from a metallic to an Anderson insulating phases with increasing Δ; (2) intermediate interaction regime for $0.87 < U < U_{c*} \approx 1.85$, where U_{c*} corresponds to the maximum interaction value of the metallic region: in this regimes for varying Δ two MITs occurs, i.e. reentrant effect of insulating phase appears; and (3) strong interaction regime for $U > 1.85$, where metallic phase does not exist, only Mott or Anderson insulating phases. Our obtained phase diagram is qualitatively consistent with those known in the literature at $T = 0$[8,9] as well as $T \neq 0$.[23] However, the phase diagram obtained from TMT-DMFT using the equation of motion method or slave boson technique as an impurity solver[9] does not include the metal–insulator coexistence region.

Now we present some results concerning conductivity in the weak and intermediate interaction regimes. We start by checking formula (10) for the case $T = 0$ and $U = 0$, i.e. for the Anderson model. In Fig. 2, we show the dc conductivity as a function of the disorder strength Δ. It can be seen that while the dc conductivity calculated from (10) within TMT-DMFT vanishes at the Anderson MIT, i.e. for $\Delta > \Delta_c \approx 1.36$, this quantity within CPA-DMFT still has a finite value, that does not agree with the phase diagram in Fig. 1. Our calculated σ_T within TMT-DMFT has a similar shape of the dc conductivity curves for a simple cubic lattice obtained in Refs. 24–26.

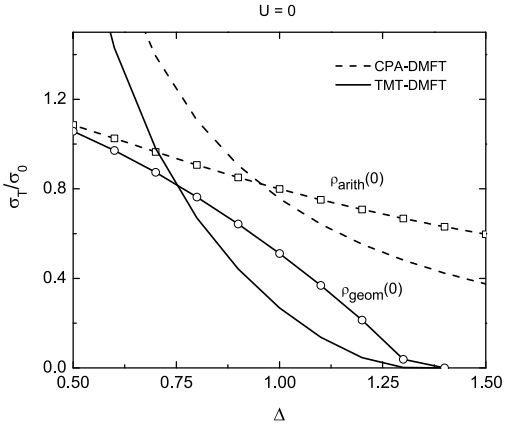

Fig. 2. TMT-DMFT and CPA-DMFT dc conductivity in the Anderson model ($U = 0$) at zero temperature as a function of the disorder strength Δ. Solid (dash) lines are calculated from (10) by using the geometrically (arithmetically) averaged Green functions. Also shown, the geometrically and arithmetically averaged LDOS at the band center ($\omega = 0$).

(i) Weak interaction regime. Figure 3 (upper panel) shows TMT-DMFT and CPA-DMFT optical conductivity when $U = 0.25$ for different values of $\Delta = 0.0, 0.75, 1.0$ and 2.1 at $T = 0.01$. For $\Delta = 0$ both approach gives the same result and indicates a metallic phase of the system. For small values of disorder ($\Delta = 0.75, 1.0$) the system is in metallic phase with the broad low frequency peak. This peak moves to higher frequency and its intensity is reduced as disorder increases. However, for the large disorder ($\Delta = 2.1$) while the low frequency peak within TMT-DMFT

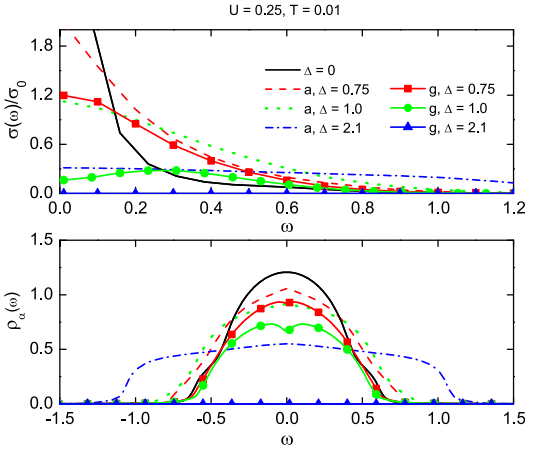

Fig. 3. (Color online) TMT-DMFT and CPA-DMFT optical conductivity (upper panel); TDOS and arithmetically averaged LDOS (lower panel) in the weak interaction regime ($U = 0.25$) at $T = 0.01$ for different values of $\Delta = 0, 0.75, 1.0$ and 2.1; a and g stand for CPA-DMFT and TMT-DMFT approaches, respectively. The Fermi level is chosen as the origin of the energy axis.

calculation disappears and the conductivity vanishes, indicating an Anderson insulating phase of the system, the CPA-DMFT conductivity remains finite, specifying a metallic phase. The TMT-DMFT results agree well with the corresponding TDOS shown in the lower panel of Fig. 3, where a suppression of TDOS at the Fermi level increases as the disorder strength increases, and followed along a vertical line at $U = 0.25$ in the phase diagram in Fig. 1. The density of states and the optical conductivity within CPA-DMFT, which take into account both extended and localized states, are bigger than the corresponding quantities within TMT-DMFT, then for $\Delta = 2.1$ they do not agree with the TMT-DMFT phase diagram. We note that within TMT-DMFT the ground state is in the Anderson insulating phase if $\int \rho_g(\omega) d\omega = 0$, i.e. $\rho_g(\omega) = 0$ for all ω, this leads to the spectral function $A_g(\varepsilon, \omega) = 0$ and the optical conductivity vanishes. We have checked the effect of the energy broadening (0^+) induced in our calculations. The results showed that in the AI phase, a decrease in 0^+ leads to a rapid reduction in conductivity values, approaching almost zero upon extrapolating 0^+ to zero at specific points verified on the phase diagram. At finite temperature, the optical conductivity in the Anderson localized phase, in our calculation, does not equal zero but very small. In fact, the effect of finite temperature can be treated by making analytical continuation $\omega \to \omega + i\delta$. The parameter δ is generally expected to be an increasing function of temperature.[3] This is a limitation of the TMT-DMFT.[27]

In our calculations, the effect of temperature on optical conductivity is relatively small and mainly occurs at the low frequency region, where it decreases with increasing temperature as shown in Fig. 4 for $U = 0.25, \Delta = 0.75$. The temperature effect on the dc conductivity is more clear. In Fig. 5, we show the TMT-DMFT dc conductivity as a function of temperature in the weak interaction regime $(U = 0.25)$ for different values of $\Delta = 0.0, 0.5, 0.75, 1.0$ and 1.5. It is seen that in this interaction regime at a fixed temperature T the dc conductivity decreases as disorder increases.

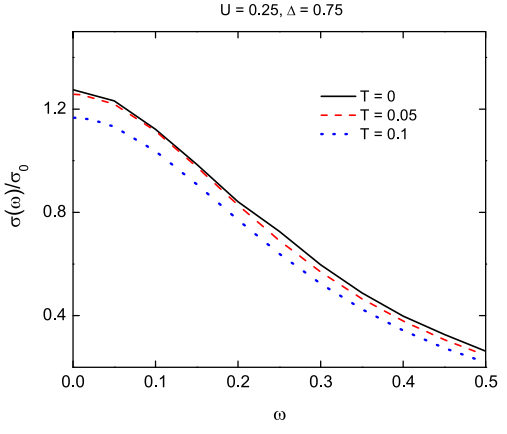

Fig. 4. (Color online) Effect of temperature on the optical conductivity for $U = 0.25$ and $\Delta = 0.75$.

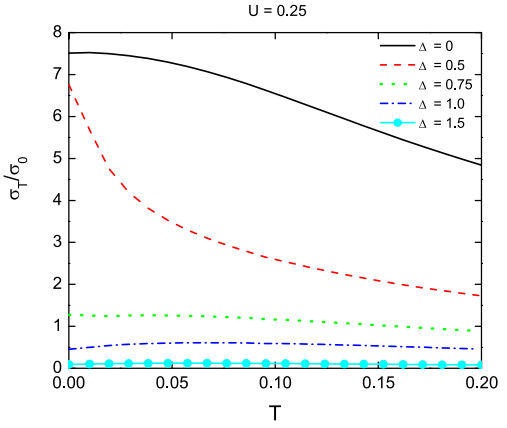

Fig. 5. (Color online) TMT-DMFT dc conductivity as a function of temperature in the weak interaction regime ($U = 0.25$) for different values of $\Delta = 0.0, 0.5, 0.75, 1.0$ and 1.5.

In addition, for a fixed and weak disorder strengths ($\Delta = 0.0, 0.5, 0.75, 1.0$) the dc conductivity decreases with increasing temperature and for large value $\Delta(\Delta = 1.5)$ near the critical disorder strength the dc conductivity is very small.

(ii) Intermediate interaction regime. Figure 6 (upper panel) displays the behavior of the optical conductivity within TMT-DMFT and CPA-DMFT approaches when $U = 1.25$ at $T = 0.01$ for various disorder strengths. For $\Delta = 0$ both approaches give the same result and indicates a Mott insulating phase of the system. It is seen that for small values of disorder ($\Delta = 0.0, 0.5$) the high frequency peak appears and the optical conductivity has a shape that is typical of a gapped insulator.

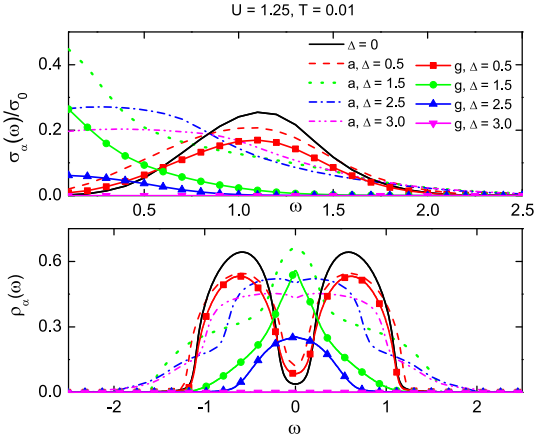

Fig. 6. (Color online) TMT-DMFT and CPA-DMFT optical conductivity (upper panel); TDOS and arithmetically averaged LDOS (lower panel) in the intermediate interaction regime ($U = 1.25$) at $T = 0.01$ for different values of $\Delta = 0.0, 0.5, 1.5, 2.5$ and 3.0; a and g stand for CPA-DMFT and TMT-DMFT approaches, respectively.

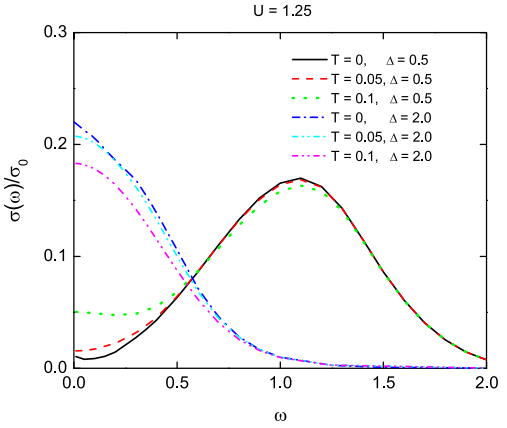

Fig. 7. (Color online) Effect of temperature on the optical conductivity for $U = 1.25$, $\Delta = 0.5$ and 2.0.

This high frequency peak is decreased as disorder increases and for the intermediate disorder ($\Delta = 1.5, 2.5$) a low frequency peak appears, indicating the system is a metal. This low frequency peak then decreases in intensity as disorder grows, and finally disappears at the critical disorder strength ($\Delta \approx 3.0$), signaling a phase transition from the metal to the Anderson insulator. Again, TMT-DMFT results agree well with the corresponding TDOS shown in the lower panel of Fig. 6 and followed along a vertical line at $U = 1.25$ in the phase diagram in Fig. 1, while that CPA-DMFT for $\Delta = 3.0$ does not agree with him. In Fig. 7, we show the influence of temperature on optical conductivity. Similar to the weak interaction regime, the temperature effect mainly occurs in the low frequency region. However, there are two different cases: with a small disorder ($\Delta = 0.5$) corresponding to the Mott insulating phase, the optical conductivity increases with temperature, while with a large disorder ($\Delta = 2.0$) corresponds to the metallic phase, the optical conductivity decreases with increasing temperature.

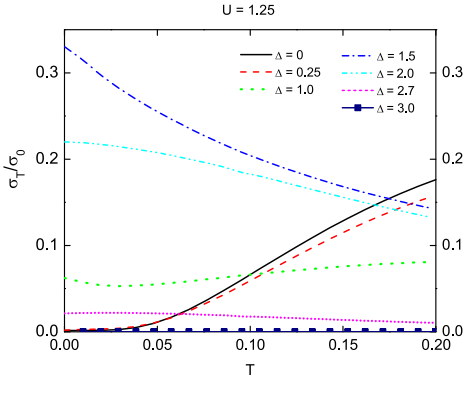

Fig. 8. (Color online) TMT-DMFT dc conductivity as a function of temperature in the intermediate interaction regime ($U = 1.25$) for different values of $\Delta = 0.0, 0.25, 1.0, 1.5, 2.0, 2.7$ and 3.0.

Figure 8 presents the evolution in the intermediate interaction regime of the TMT dc conductivity as a function of temperature with disorder when $U = 1.25$. One can see that the activated conductivity occurs in the Mott state at low disorder ($\Delta = 0.0, 0.25$), then it changes to a metallic behavior with increasing disorder ($\Delta = 1.0, 1.5, 2.0, 2.7$). Finally, the dc conductivity reduces and vanishes in the Anderson localization regime at high disorder intensity ($\Delta = 3.0$). Our results on TMT dc conductivity in Fig. 8 are consistent with those on optical one in Fig. 6. They all provide evidence for the metal–insulator transitions in the system as the strength of the disorder is varied. The similar picture has been observed in the AFK model at half-filling.[7]

4. Conclusion

In summary, we for the first time studied the conductivity of the half-filled disordered Hubbard model by using a typical medium dynamical mean field theory with equation of motion method as an impurity solver. We found that our TMT dc conductivity for $U = 0$ is consistent with those known in the literature[24–26] and the calculated optical and dc conductivity for different cases are in agreement with the corresponding TDOS and the obtained phase diagram. In the weak interaction regime at a fixed temperature the optical conductivity in low frequencies and the dc conductivity decrease as disorder strength increases, while in the intermediate interaction regime, the results show reentrant effect of the insulating phase, i.e. the disorder can make the system more metallic, that in agreement with the experiments on disordered correlated systems.[16] In addition, in both interaction regimes the dc conductivity near Anderson MIT is very small.

The advantages of EOM are fast computational time and spectral functions directly on the real frequency axis. However this method is more reasonable at high temperatures, therefore more exact impurity solvers within TMT-DMFT as well as more sophisticated approaches beyond him need to be applied to find more accurate results on this topic.

Acknowledgments

This research is funded by the National Foundation of Science and Technology Development (NAFOSTED) under Grant No. 103.01–2020.20 and the International Center of Physics at the Institute of Physics, Vietnam Academy of Science and Technology under Grant ICP.2022.01.

References

1. D. M. Basko, I. L. Aleiner and Altshuler, *Ann. Phys.* (New York) **321** (2006) 1126.
2. K. Byczuk, W. Hofstetter and D. Vollhardt, *Int. J. Mod. Phys. B* **24** (2010) 1727.
3. V. Dobrosavljevic, *Int. J. Mod. Phys. B* **24** (2010) 1680.
4. A. Georges, G. Kotliar, W. Krauth and M. J. Rozenberg, *Rev. Mod. Phys.* **68** (1996) 13.

5. V. Dobrosavljevic, A. A. Pastor and B. K. Nikolic, *Europhys. Lett.* **62** (2003) 76.
6. K. Byczuk, *Phys. Rev. B* **71** (2005) 205105.
7. R. D. B. Carvalho and M. A. Gusmao, *Phys. Rev. B* **87** (2013) 085122.
8. K. Byczuk, W. Hofstetter and D. Vollhardt, *Phys. Rev. Lett.* **94** (2005) 0564021.
9. M. C. O. Aguiar, V. Dobrosavljevic, E. Abrahams and G. Kotliar, *Phys. Rev. Lett.* **102** (2009) 156402.
10. A. T. Hoang, T. H. Y. Nguyen and D. A. Le, *Physica B* **570** (2019) 320.
11. A. T. Hoang, T. H. Y. Nguyen and D. A. Le, *Mod. Phys. Lett. B* **35** (2021) 2150357.
12. T. H. Y. Nguyen, D. A. Le and A. T. Hoang, *New J. Phys.* **24** (2022) 053054.
13. X. Chen and R. J. Gooding, *Phys. Rev. B* **80** (2009) 115125.
14. P. B. Chakraborty, K. Byczuk and D. Vollhardt, *Phys. Rev. B* **84** (2021) 035121.
15. N. D. Patel, A. Mukherjee, N. Kaushal, A. Moreo and E. Dagotto, *Phys. Rev. Lett.* **119** (2017) 086601.
16. M. M. Radonjic, D. Tanaskovic, V. Dobrosavljevic and K. Haule, *Phys. Rev. B* **81** (2010) 075118.
17. H. Barman, M. S. Laad and S. R. Hassan, *J. Phys.: Condens. Matter* **30** (2018) 195603.
18. Y. Meir, N. S. Wingreen and P. A. Lee, *Phys. Rev. Lett.* **66** (1991) 3048.
19. Q. Feng, Study of single impurity Anderson model and dynamical mean field theory based on equation of motion method, Dissertation zur Erlangung des Doktorgrades der Naturwissenschaften, Chap. 2, Goether Universitat Frankfurt in Frankfurt am Main (2009), pp. 19–20.
20. D. Semmler, K. Byczuk and W. Hofstetter, *Phys. Rev. B* **84** (2011) 115113.
21. T. H. Y. Nguyen and A. T. Hoang, *J. Phys.: Conf. Ser.* **2485** (2023) 012004.
22. M. Jarrel, J. K. Freericks and T. Pruschke, *Phys. Rev. B* **51** (1995) 11704.
23. H. Braganca, M. C. O. Aguiar, J. Vučičević, D. Tanasković and V. Dobrosavljević, *Phys. Rev. B* **92** (2015) 125143.
24. E. N. Economou, C. M. Soukoulis and A. D. Zdetsis, *Phys. Rev. B* **31** (1985) 6483.
25. I. Sadakata, *J. Phys. Soc. Jpn.* **55** (1986) 3991.
26. E. Kolley and W. Kolley, *J. Phys. C: Solid State Phys.* **B21** (1988) 6099.
27. Y. Song, W. A. Atkinson and R. Wortis, *Phys. Rev. B* **76** (2007) 045105.